Composite Structures 164 (2017) 32–42

Contents lists available at ScienceDirect

Composite Structures

journal homepage: www.elsevier.com/locate/compstruct

Influences of CNT dispersion and pore characteristics on the electrical performance of cementitious composites

G.M. Kim [a,1], B.J. Yang [b,1], K.J. Cho [a], E.M. Kim [a], H.K. Lee [a,*]

[a] Department of Civil and Environmental Engineering, Korea Advanced Institute of Science and Technology (KAIST), 291 Daehak-ro, Yuseong-gu, Daejeon 34141, Republic of Korea
[b] Multifunctional Structural Composite Research Center, Institute of Advanced Composite Materials, Korea Institute of Science and Technology (KIST), 92 Chudong-ro, Bongdong-eup, Wanju-gun, Jeonbuk 55324, Republic of Korea

ARTICLE INFO

Article history:
Received 13 April 2016
Revised 1 December 2016
Accepted 9 December 2016
Available online 19 December 2016

Keywords:
Cementitious composites incorporating CNT
Electrical conductivity
Air porosity
CNT dispersion
Micromechanics-based modeling

ABSTRACT

In the present study, cementitious composite incorporating a carbon nanotube (CNT) with highly improved electrical conductivity comparable to that of a semiconductor is developed and investigated. The CNT and pore characteristics within a cementitious matrix are considered as the most influential factors which determine the overall performance of the material, and these factors are artificially controlled by incorporating silica fume and a superplasticizer. Additionally, a micromechanics-based model is proposed to predict the electrical performance and percolation threshold of the composites. A parametric study based on the developed model is conducted, and the influences of the constituent properties on the overall electrical characteristics of composites are discussed. The effectiveness of the proposed hypothesis is demonstrated by comparing it to the experimental results in the present study and from the previous work.

1. Introduction

In recent years, the need for high-performance multifunctional construction materials has increased consistently in civil engineering fields [1]. Cementitious material is the third most commonly consumed material after fossil fuels and food crops [2], and the functionality of the cementitious materials is therefore expected to have a considerable impact on numerous industrial fields [3]. Carbon nanotube (CNT), a typical nanotechnology-based product, has outstanding mechanical, electrical, and thermal properties that render it an ideal material for improving the performance of cementitious composites [4–6,45]. However, although the attractive properties of nano-materials have led to intensive research, relatively little work has been reported on the use of novel materials in construction material sciences [7]. Especially, prior work on cementitious composites incorporating CNT generally focused on their mechanical characteristic.

Chaipanich et al. (2010) conducted an experimental study to improve the compressive strength of the cement-based composites by incorporating CNT and fly ash into them [8]. It was found that the utilization of CNT resulted in higher compressive strength of fly ash mortar and that the highest strength can be obtained when CNTs and fly ash contents were 1.0% and 20.0% by weight of binder materials, respectively [8]. The interactions among the CNTs, fly ash, and cement matrix were also analyzed using scanning electron (SEM) micrographs, showing that CNT acted as a strengthening filler material in the cement mortar [8]. In addition, an effective dispersion method of carbon nanotube (CNT) in cement materials was proposed by Konsta-Gdoutos et al. [9]. It was reported that the dispersion level can be improved by applying ultrasonic energy in combination with the use of a surfactant, and the mechanical characteristics of composites increased through proper dispersion of nanotubes [9].

More recently, it has been reported that the addition of CNT to the cementitious composite can improve the electrical, thermal, damping and fracture properties [10,11]. In addition, the composites can be used as a sensing, electromagnetic interference, smoke detection materials and so on [10]. The electrical performances of cementitious composites incorporating CNT were investigated by Azhari and Banthia (2012) [12]. The ability to sense an applied compressive load was experimentally tested, with the results indicating that the developed composites have the potential to be used as sensors for detecting microcracks in concrete [12]. Singh et al. (2013) tested the electromagnetic interference (EMI) shielding effectiveness (SE) of cement composites incorporating CNT [13]. The addition of 15.0 wt% nanotubes in the cementitious material

* Corresponding author.
E-mail address: haengki@kaist.ac.kr (H.K. Lee).
[1] These authors contributed equally to this work.

http://dx.doi.org/10.1016/j.compstruct.2016.12.049
0263-8223/

exhibited a good SE in the X-band range; the SE was found to be dominated by the absorption properties [13]. The surface interaction and morphology of the composites were also explored through XRD, SEM, and X-ray techniques [13]. Kim et al. (2014) investigated the effects of the addition of silica fume on the electromechanical characteristics of cementitious composites incorporating CNT, and various experimental tests including compressive strength, electrical resistance, and SEM image analysis were conducted in the study [14].

In the present study, cementitious composites incorporating CNT with high electrical conductivity comparable to that of a semiconductor ($10–10^5$) are developed by the incorporation of CNT [15]. To investigate the effects of the CNT dispersion and the pore characteristics on the performance of cementitious composites, numerous specimens with different amounts of silica fume and a superplasticizer are produced. In addition, experimental evaluations of the compressive strength and electrical properties of the fabricated composites are carried out, and the microstructures and pore distributions of the composites are analyzed through SEM and mercury intrusion porosimetry (MIP) methods.

A theoretical model based on micromechanics [15,17] is also proposed to predict the electrical conductivity of the cementitious composites incorporating CNT. The pores in the matrix are taken into account through a two-level homogenization process, and the CNT agglomerates are assumed to be determined by the curviness of the CNTs. The interface properties between the CNT and the matrix are also represented by imperfectly bonded inclusions from a theory proposed by Duan and Karihaloo (2007) [18]. Lastly, the effectiveness of the proposed analytical model is proved by comparing experimental results from the present study to those in the previous works [19,20].

2. Experimental procedure

2.1. Materials

The CNT (Hyosung Inc.) used in the present study were produced by means of thermal chemical vapor deposition (CVD) and were purified beyond 95.0%. It is well known that the main impurities during the CVD process are carbonaceous materials and catalysts used for the production [21]. The diameter of the CNT ranged from 12.0 nm to 40.0 nm, and the length were approximately 10.0 μm. Type 1 Portland cement and silica fume were utilized as binder materials. A poly-carboxylic acid-based superplasticizer (GLENUIM 8008, BASF Pozzolith, Ltd.) was used to improve the workability and to disperse CNT in the cementitious matrix.

Table 1 shows the mix proportion of the cementitious composites incorporating CNT. Five types of specimens were prepared, and a specimen which was only composed of cement paste was labeled as the control specimen. For all specimens, the water/cement (w/c) ratio was fixed at 0.3, and CNT at an amount of 0.5% by weight of cement were added to the composite specimens (C-CNT, P-CNT, F-CNT, and PF-CNT). In addition, silica fume and a superplasticizer in corresponding amounts of 20.0 wt% and 1.6 wt%, respectively, were applied. The density of the material composition utilized in the present study is given in Table 1.

The detailed specimen notation method according to the combination of the material compositions is illustrated in Fig. 1(a). The fabrication processes of the specimens were as follows: dry materials (two or three selected from the cement, the silica fume, and the CNT) were mixed for 1 min using a standard Hobart mixer, and then further mixed for another 5 min after the superplasticizer and water were added to the mixtures. The fresh mixtures were cast into a cubic mold $50 \times 50 \times 50\ mm^3$ in size. A tamper was used to compact the mixture. The specimens were then sealed to prevent the evaporation of water. After 1 day of curing, the specimens were demolded and cured in the sealed condition for 28 days at 20 ± 5 °C. To measure the resistance of the hardened specimens, electrodes were designed in equivalent planes using silver paste to minimize the contact resistance between the composite matrix and the electrodes [14,22]. These had a width and height of 10 mm and 20 mm, respectively (Fig. 1(b)).

2.2. Test methods and procedures

The electrical resistance of the composite specimens was measured using a digital multimeter (Agilent Technologies 34410A), and the resistivity (Ω·m) was calculated according to Eq. (1), as follows [23],

$$\rho = R \cdot \frac{A}{L} \tag{1}$$

where ρ is the resistivity (Ω·m) and R is the measured resistance (Ω). L and A denote the spacing between the electrodes (m) and the cross-section of an electrode on a composite specimen (m^2), respectively. A polarization effect increases the electrical resistivity of the composites when the CNT are not uniformly dispersed in the cementitious matrix [24]. The electrical resistance measured within 1 s to exclude the effect of the polarization [23]. The electrical resistance of the composites was measured at 3, 7, 14, and 28 curing days to investigate how much it changed during the hydration process. The hardened specimen cured for 28 days was then subjected to a compressive strength test based on ASTM C 109 with the use of a 3000 kN universal testing machine (UTM) with a cross-head speed of 0.02 mm/s [25]. In addition, MIP and SEM tests were conducted to analyze the microstructures of the cementitious composites incorporating CNT. The MIP test for investigating the correlation between the CNT dispersion and distribution of pores was carried out with a porosimeter (Auto pore IV 121 9500, Micrometritics Instrument Co.), which can detect pore diameters in a range of 0.003–10 μm. The contact angle and surface tension in the test were 130° and 0.485 N/m, respectively [26]. For the SEM analysis (Nova NanoSEM 230, FEI CO.; S-5000, Hitachi Co.), the composite specimen was dried in an oven at 50 °C for 12 h and then coated with gold under a low vacuum [14].

2.3. Results and discussion

The experimental results of electrical resistivity and compressive strength corresponding to each specimen are shown in Fig. 2 (a) and (b). It was found that the addition of CNT reduced the electrical resistivity in all cases. In particular, the electrical resistivity of the PF-CNT specimen was reduced by more than 1000 times compared to that of control specimen. The electrical resistivity of the C-CNT, P-CNT and F-CNT specimens was relatively higher than that of PF-CNT specimen. However, the electrical resistivity of the P-CNT specimen was slightly lower than those of C-CNT and F-CN specimens. Meanwhile, the electrical resistivity of the PF-CNT and F-CNT specimens was almost unchanged as the curing days increased, while those of C-CNT and P-CNT specimens increased. The evaporation of water can significantly change the electrical resistivity of cementitious composites [22]. Silica fume added to the PF-CNT and F-CNT can densify the matrix and reduce the evaporable water in the composite matrix [14]. That is, the electrical resistivity of PF-CNT and F-CNT specimens in the present study was not significantly affected by the evaporation of the water.

The compressive strengths of C-CNT and P-CNT specimens were slightly less than that of the control specimen. In contrast, the compressive strength of the F-CNT specimen were approximately 2 times higher than that of control specimen. The improvement of compressive strength on the F-CNT specimen was possibly

Table 1
Mix proportion expressed in terms of mass ratio and total porosity of the cementitious composites incorporating CNT.

Specimen	Cement (3.10)*	Water (1.00)	CNT (1.32)	Silica fume (2.10)	Super-plasticizer (1.07)	Total porosity (%)
Control	100	30	0.0	0.0	0.0	14.03
C-CNT			0.5	0.0	00.0	16.00
P-CNT			0.5	0.0	1.6	21.31
F-CNT			0.5	20.0	0.0	9.78
PF-CNT			0.5	20.0	1.6	12.68

* Specific gravity of materials.

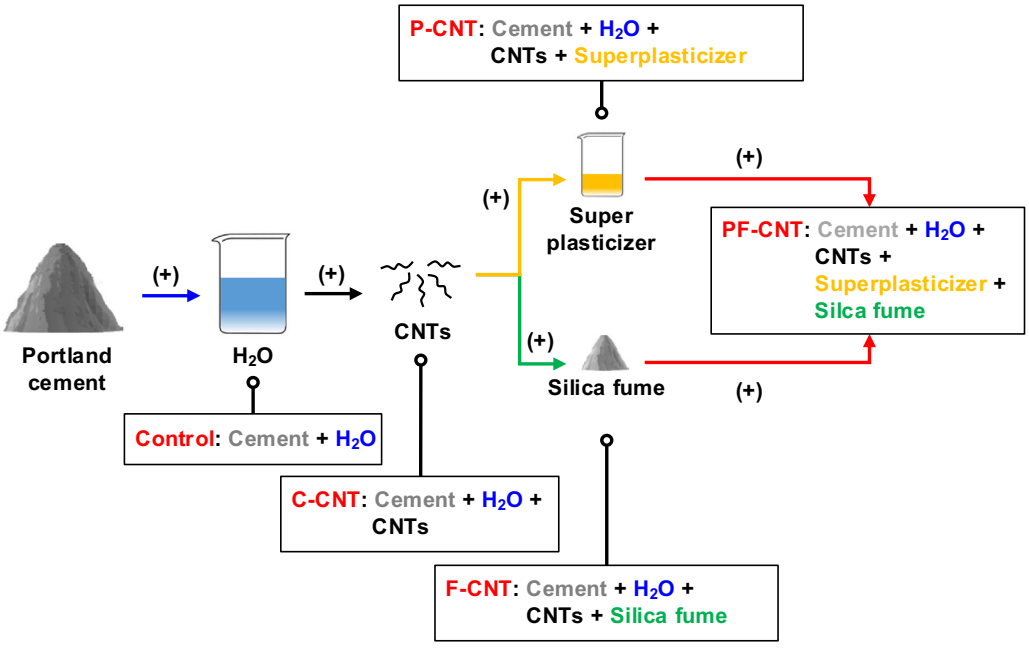

(a)

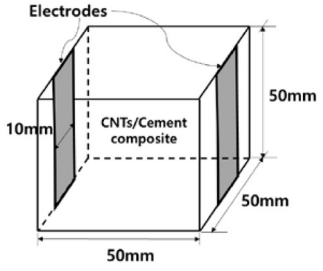

(b)

Fig. 1. (a) A schematic of the mixing procedure of cementitious composite incorporating CNT, and (b) an illustration of the composite specimen with a silver paste electrode.

caused by the addition of silica fume [27]. Toutanji and El-Korchi (1995) reported that the addition of silica fume improved the compressive strength of cementitious materials [27]. The compressive strength of PF-CNT specimen was a slightly higher compared to that of F-CNT specimen. The increase in the compressive strength of the PF-CNT specimen may be attributed to bridging effect of CNT, which can be generated when CNT is well dispersed in the cementitious matrix [14]. In addition, silica fumes in PF-CNT specimen possibly anchor CNTs, thereby improving the bond strength between CNTs and hydrates in cementitious matrix [14].

The total porosity and pore size distribution (PSD) of cementitious composites incorporating CNT as measured by the MIP tests is represented in Table 1 and Fig. 3(a). In addition, SEM images of all composite specimens are shown in Fig. 3(b)–(e) in the following order: the C-CNT, P-CNT, F-CNT, and PF-CNT specimens. In this section, the most significant characteristics of each specimen are addressed, after which the results of a comprehensive analysis of the experimental study are summarized.

First, for the control specimen, the porosity with diameters of 0.01–0.05 μm was 46.9%, as shown in Fig. 3(a). In contrast, the porosity with diameters of 0.01–0.05 μm in the C-CNT specimen reduced up to 27.5%. In addition, the porosity with diameters of 0.10–10.00 μm in the C-CNT specimen increased by more than four times in comparison of the control specimen (Fig. 3(a)). Fig. 3(b)

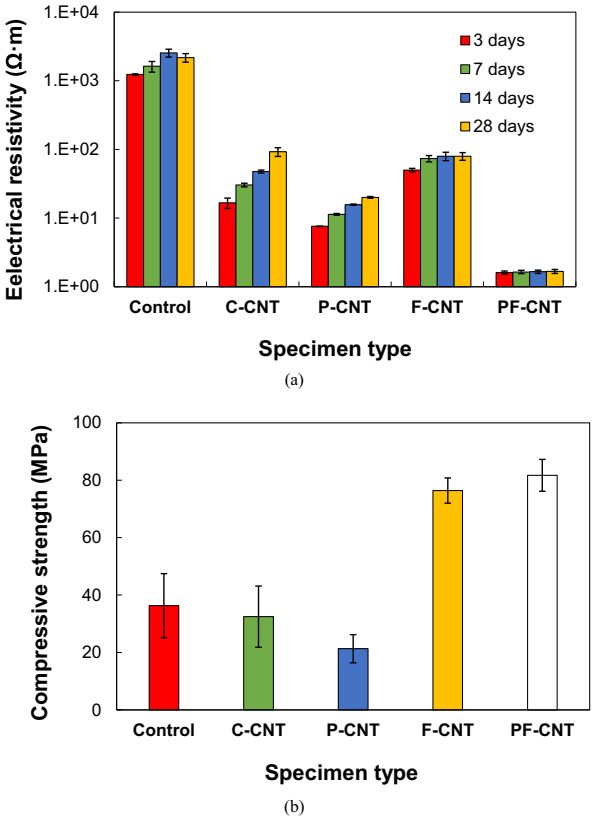

Fig. 2. (a) Electrical resistivity of cementitious composites incorporating CNT at 3, 7, 14, and 28 days of curing, and (b) test results of the 28-day compressive strength of the specimens.

shows a number of floccuslike CNT agglomerates spread over the C-CNT specimen. The agglomeration of CNT in the C-CNT specimen increased the electrical resistivity compared to PF-CNT. In addition, the agglomerates of CNT readily entrap water molecules which in turn is most likely transformed into pores after evaporation of the water [22]. The entrapped water is responsible for an increase in the total porosity of C-CNT specimen compared to that of control specimen [28]. However, a further study is necessary to investigate the effect of entrapped water in CNT agglomerates on the total porosity of the composites and means of controlling its amount.

The total porosity of the C-CNT specimen in Table 1 was 16.00%, while that of control was 14.03%. The increase in the total porosity led to the reduction in the compressive strength of the C-CNT specimen compared to the control specimen [29]. Furthermore, the increase in the total porosity is responsible for the variation of the electrical resistivity in the C-CNT specimen during 28 days of curing. The increase in the total porosity probably degrades the continuity of CNT particles and increases the influence of pore solution on the electrical resistivity of the composites incorporating CNT [22].

Similarly, the porosity with diameters of 0.01–0.05 μm in the P-CNT specimen was approximately two times lower than that in the control specimen (see Fig. 3(a)). In addition, the porosity with diameters of 1.00–10.00 μm in the P-CNT specimen was nine times higher than that in the control specimen. Table 1 shows that the total porosity of the P-CNT specimen (21.31%) increased by more than 6% in comparison with the control specimen (14.03%). Meanwhile, Fig. 3(c) shows that the CNT particles in the P-CNT specimen was agglomerated. The pore characteristics and CNT dispersion states was almost similar to the C-CNT specimen. However, the agglomeration extent of CNT for the P-CNT specimen is less than that for the C-CN and F-CNT specimens in Fig. 3(b)–(d). That is, the lower electrical resistivity of the P-CNT specimen in comparison with those of the C-CNT and F-CNT specimens may be attributed to the reduction of van der Waals attractive force among CNT particles resulted from the use of superplasticizer, leading to a slight improvement of CNT dispersion [30].

For the F-CNT specimen, which is mixed with silica fume, the porosity with diameters of 1.0–10.00 μm is reduced compared to C-CNT and P-CNT specimens, while that with diameters of less than 0.01 μm greatly increased (see Fig. 3(a)). According to Feldman and Cheng-Yi, (1985), silica fume added to a cementitious matrix leads to a transformation of a large pore (>1.0 μm) into a small pore (<0.01 μm) and to a reduction in the total porosity [31]. The total porosity of the F-CNT specimen was 9.78%, while that of control specimen was 14.03%. The change in pore characteristics resulted from the addition of silica fume improved the compressive strength of the F-CNT specimen [14]. Meanwhile, CNT agglomerates were observed in the F-CNT specimen as shown Fig. 3(d), meaning that the simple addition of silica fume is not an effective way to improve the dispersion of CNT particles in cementitious matrix. However, silica fume in the cementitious matrix can inhibit the formation of a large pore and an increase in the total porosity of the composites [31]. The change in the pore characteristics possibly mitigated the variation of electrical resistivity of the F-CNT specimen. That is, the reduction in the total porosity and the transformation of a large pore into a small pore reduced the influence of the pore solution on the electrical resistivity of the F-CNT specimen.

The PSD of PF-CNT is similar to the F-CNT specimen, as shown in Fig. 3(a). For the PF-CNT specimen, the porosity with diameters of 1.0–10.00 μm is lower than that of the C-CNT and P-CNT specimens, while the porosity with diameters of less than 0.01 μm increased dramatically. Fig. 3(e) shows that the CNT particles in PF-CNT specimen were well dispersed. A schematic description of the enhanced electrical resistivity of the PF-CNT specimen is presented in Fig. 4. First, the distances between CNT particles increased by the incorporation of a superplasticizer, which reduces the attractive force among them [32]. The silica fume then fills the gap regions between the CNTs, thereby increasing the distances between them. Kim et al. (2014) observed that silica fume particles in a cementitious composite incorporating CNT were settled down at the interfacial gaps between CNTs [14]. Another influence of the addition of silica fume was presented in Fig. 4(b). Large pores in cementitious matrix can provide the place which is filled with pore solution. It seems that the pore solution in CNT-incorporated cementitious composites without silica fume served as a part of temporary conductive pathway. As the pore solution evaporated over a period of time, the continuity level of the conductive pathway degraded, leading an increase in the electrical resistivity of the composites [23]. In contrast, the addition of silica fume significantly decreased a large pores which in turn possibly reduced the contribution of pore solution to electrical resistivity. That is, the continuity level of conductive pathways in the composites may be improved when silica fume added, which reduced the variation of electrical resistivity.

3. Numerical predictions

3.1. Micromechanics-based model for CNTs-reinforced cementitious composites

Based on the experimental observations in the previous section, it was found that the electrical properties of the cementitious composite are quite sensitive to the degrees of porosity and CNT

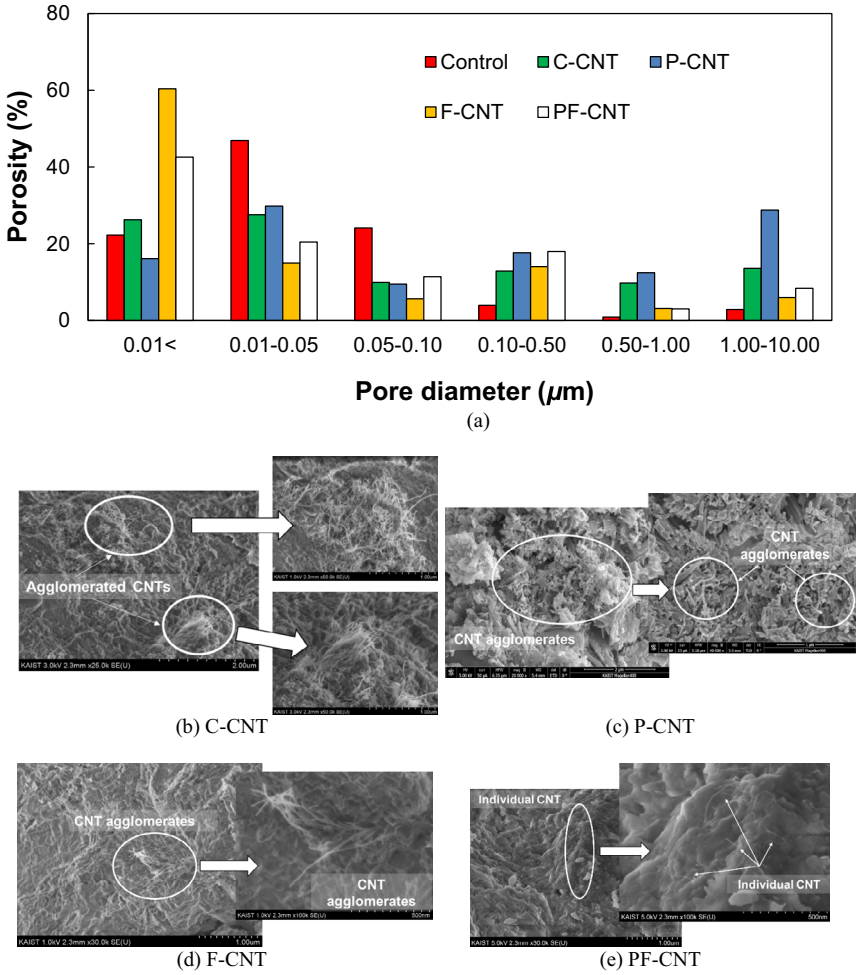

Fig. 3. (a) MIP test results of the cementitious composites incorporating CNT, and SEM images of (b) C-CNT, (c) P-CNT, (d) F-CNT, and (e) PF-CNT.

agglomeration. To consider the key factors in a theoretical model, a two-level homogenization process (Fig. 5) based on micromechanics is proposed in this study. The first homogenization process is one in which the silica fume, pores, and cement are treated as a single matrix material. In this case, the following two assumptions are made: first, the electrical conductivity of the silica fume and cement are approximately equal [33,34], and second, the shape of the silica fume and porosity can be represented as a spherical particle [35].

With these assumptions, the electrical conductivity of a two-phase matrix can be estimated using the Mori-Tanaka (MT) method, which is the simplest but most effective model, as follows [36,16]:

$$\sigma_m = \sigma_c + \frac{\phi_v \sigma_c T_1}{1 - \phi_v\{1 + \sigma_c T_1/(\sigma_c - \sigma_v)\}} \tag{2}$$

with

$$T_1 = 3 - \frac{9\sigma_c}{2\sigma_c + \sigma_v} \tag{3}$$

where σ_m, σ_c, and σ_v denote the electrical conductivity of the matrix, the cement, and the pores, respectively, and ϕ_v represents the volume fraction of a pore. The effective medium method is then considered for the second homogenization of the cementitious composites incorporating CNT since the MT method is not suitable for predicting the electrical behaviors of composites containing ellipsoidal inclusions [37,17]. The effective electrical conductivity of the CNT-embedded cementitious composites can be estimated by the equation below [17,46].

$$\frac{3\phi_m(\sigma_m - \sigma_e)}{\sigma_m + 2\sigma_e} + \frac{\phi_{cnt}}{3}\left\{\frac{2(\sigma_{11} - \sigma_e)}{\sigma_3 + (\sigma_{11} - \sigma_e)S_{11}} + \frac{2(\sigma_{33} - \sigma_e)}{\sigma_e + (\sigma_{33} - \sigma_e)S_{33}}\right\} = 0 \tag{4}$$

Here, σ_e is the effective electrical conductivity of the composites, σ_{11} and σ_{33} are the conductivity of the CNTs in the transverse and axial direction, respectively (Fig. 6(a)), and ϕ_m and ϕ_{cnt} correspondingly denote the volume fraction of the matrix and nanotubes, respectively. In addition, S_{11} and S_{33} are the components of the Eshelby's tensor for an ellipsoidal inclusion, as defined by Landau et al. (1984) [38].

Eq. (4) is derived based on the assumption of straight nanotubes (Fig. 6(b)); however, in reality, CNTs embedded in a cement matrix are observed to be wavy, as shown in SEM images (Fig. 3). It is caused by the inhomogeneity of cementitious material and the high aspect ratio of CNTs [39,47], and the curviness mechanism can affect the agglomeration of nanotubes [40]. Hence, in the present micromechanics-based model, the shape of a nanotube is assumed to be a sine function with a variable θ, which is the angle between the x-axis and the CNT. The wavy CNT form is then described as the cosine function with a range of one period [41]:

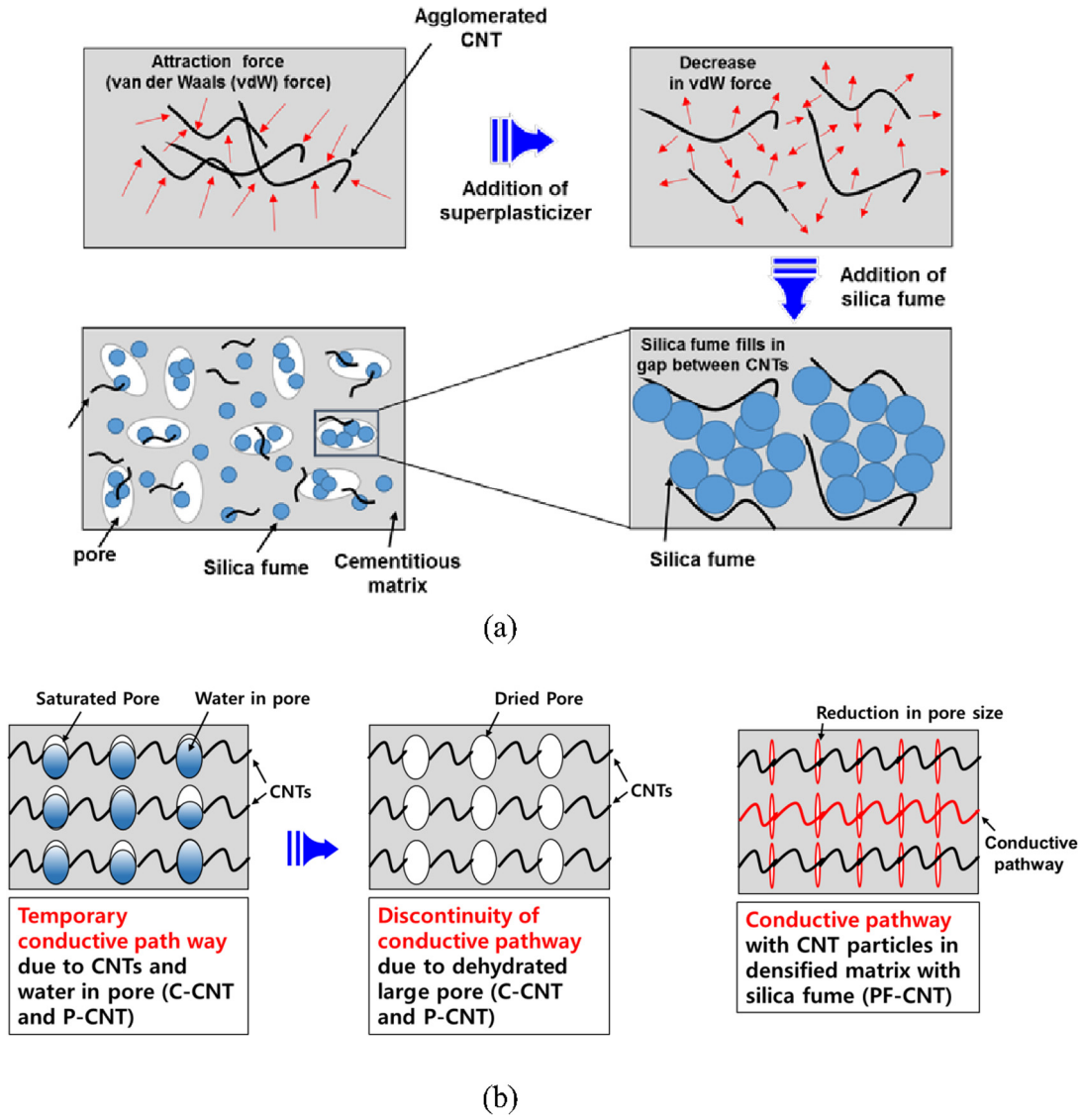

Fig. 4. Detailed analysis for the enhanced behaviors of PF-CNT: (a) influences of superplasticizer and silica fume on the dispersion of CNT and (b) the improved continuity of CNT particles by addition of silica fume.

$$y = \cos(x \cdot \tan\theta) \tag{5}$$

The length of nanotube (L) can be calculated by integrating Eq. (6), as [41,48].

$$\int_0^{\frac{2\pi}{\tan\theta}} \sqrt{dx^2 + dy^2} = \int_0^{\frac{2\pi}{\tan\theta}} \sqrt{1 + [\tan\theta\{-\sin(x \cdot \tan\theta)\}]^2}\,dx = L(\theta) \tag{6}$$

Here, the calculation result of $L(\theta)$ should be identified with L, and Eq. (5) can be expressed as:

$$y = \frac{L}{L(\theta)} \cos\left(\tan\theta \cdot \frac{xL(\theta)}{L}\right) \tag{7}$$

and the effective length of CNT (L') in Fig. 6(c) can be calculated by

$$L' = \frac{2\pi}{\tan\theta \cdot L(\theta)} \tag{8}$$

The effective CNT diameter (D') is defined as half of the length of a wavy nanotube ($2D'$), as the opposite direction of the wavy CNT (upper side) remains unaffected by the curviness (Fig. 6(c)). Thus, the effective diameter (D') and aspect ratio (α') of wavy CNTs are considered in this study. These are defined as follows:

$$D' = \frac{D}{2} + \frac{L}{L(\theta)},\ \alpha' = L'/D' = \frac{4\pi \cdot L}{\{2L + D \cdot L(\theta)\} \cdot \tan\theta} \tag{9}$$

Furthermore, the interface characteristic between the CNTs and the cement matrix is considered in the present study for a more precise prediction. By assuming that CNTs are thinly coated with an interface region, the electrical conductivity of the CNTs can be expressed by (Fig. 6(d)) [17,42,43].

$$\sigma_{ii}^c = \frac{\sigma_{ii}}{1 + \rho_i \sigma_{ii} S_{ii}(1/\alpha + 2)/R} \tag{10}$$

where ρ_i signifies the interfacial resistivity; σ_{ii} denotes the electrical conductivity of CNTs in i-axis; S_{ii} is components of the Eshelby's tensor; α and R represent the aspect ratio and the radius of CNT, respectively. The interface effect can be considered in the present study by replacing σ_{ii} with σ_{ii}^c (i = 11 and 33) in Eq. (4) [18,42,43].

The interfacial resistivity between CNTs and the matrix is modeled by a modified conductivity for the coated ellipsoidal inclusions proposed by [18,42]. Following Nan and Duan's approaches [18,42], the interphase layer is diminishingly small compared to the radius of CNT and can replace the interphase with an interface. In the limiting case that the thickness t is approximately equal to

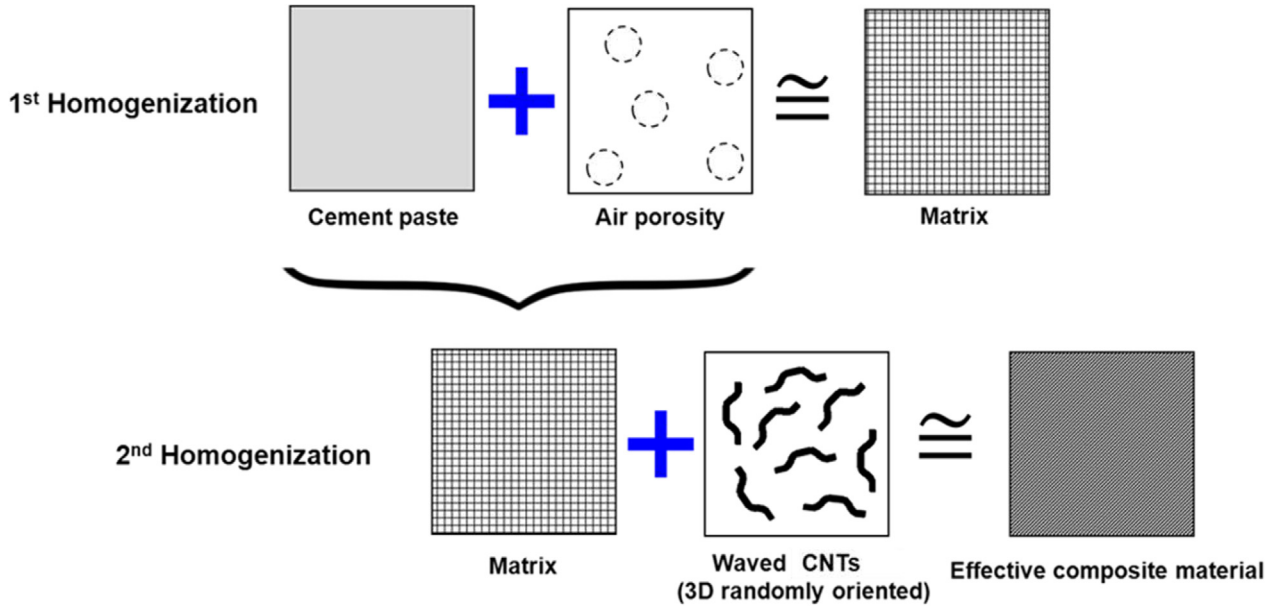

Fig. 5. Schematic representation of the two-level homogenization scheme.

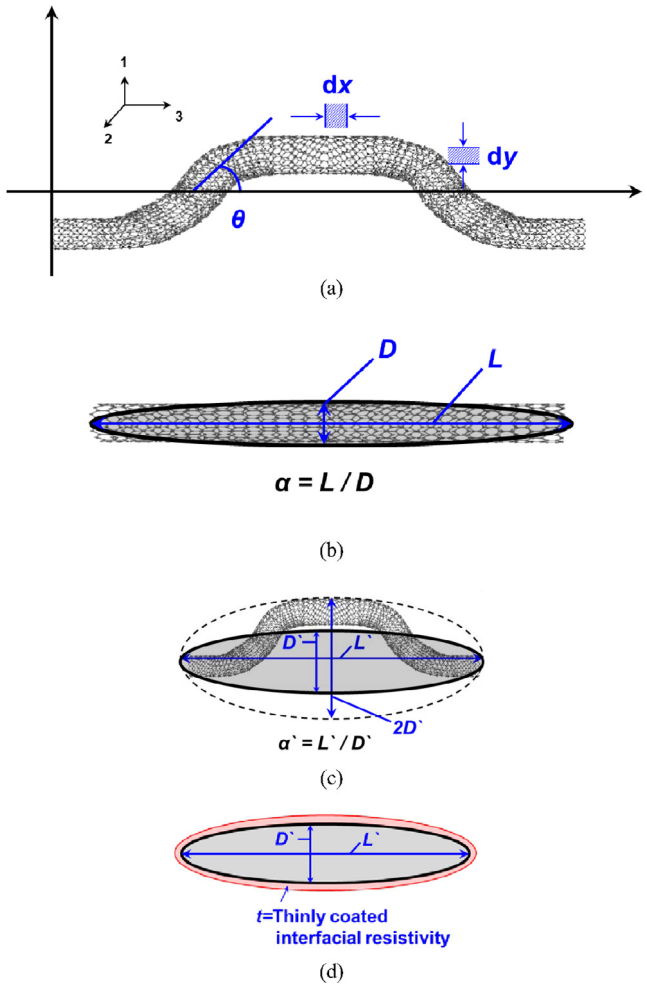

Fig. 6. Schematic representations of (a) CNT waviness as considered in this study, (b) aspect ratio of a straight nanotube, (c) effective aspect ratio of a wavy nanotube, and (d) waved nanotube with the interfacial resistivity effect.

zero, the coated CNTs and the original CNT share the same shape of S_{ii} tensor [17]. In addition, it is reported that the interface conductivity (σ_{ii}^{int}) is much lower than the intrinsic conductivity of CNTs (σ_{ii}) [13,16], therefore, it can be also assumed that $\sigma_{ii}^{int}/\sigma_{ii} \approx 0$ [18]. The thinly coated CNT with an interface region in Eq. (10) is derived based on the abovementioned considerations, and the detailed derivation processes are given in [18,42]. Further, the similar methods have been applied in many cases for estimating the electrical conductivity of nanocomposites, and its effectiveness has been validated in [17,37,43,44].

3.2. Numerical simulations and experimental comparisons

For practical engineering applications, it is desirable for the proposed model to be numerically evaluated. A series of parametric studies is, therefore, conducted while varying the material and model constants. These simulation results are presented in Fig. 7. For convenience, we adopt the same material parameters for the cementitious composites incorporating CNT as those in the present experimental study. These are: $L = 10$ μm, $D = 26$ nm; $\sigma_v = 5{\cdot}10^{-15}$ S/m, $\sigma_c = 5.72{\cdot}10^{-14}$ S/m, and $\sigma_{33} = 1.94{\cdot}10^{4}$ S/m. In addition, the electrical conductivity of the CNTs in the transverse direction (σ_{11}) is substantially lower than the axial conductivity (σ_{33}); this relationship is expressed as $\sigma_{11} = \sigma_{33}/1000$ [17].

The effects of varying the air porosity (ϕ_v) on the electrical behaviors of the matrix and composites are illustrated in Fig. 7 (a) and (b), respectively. These figures show that the increase in the volume fraction of the pores leads to lower electrical performance, especially in the case of the matrix material. For cementitious composites, the influence of the porosity begins to decrease after the percolation threshold, tending to become insignificant as the air porosity increases. In addition, the effects of CNT waviness are numerically evaluated in Fig. 7(c) and (d). The calculations show that the effective length of the wavy CNTs exponentially decreases with an increase in θ and that the waviness of the CNTs plays an important role in the electrical performance of the cementitious composites. In Fig. 7(d), the volume fraction of the porosity is fixed at $\phi_v = 10\%$.

Fig. 7(e) shows that the overall conductivity and percolation threshold of the cementitious composites improve as the CNT

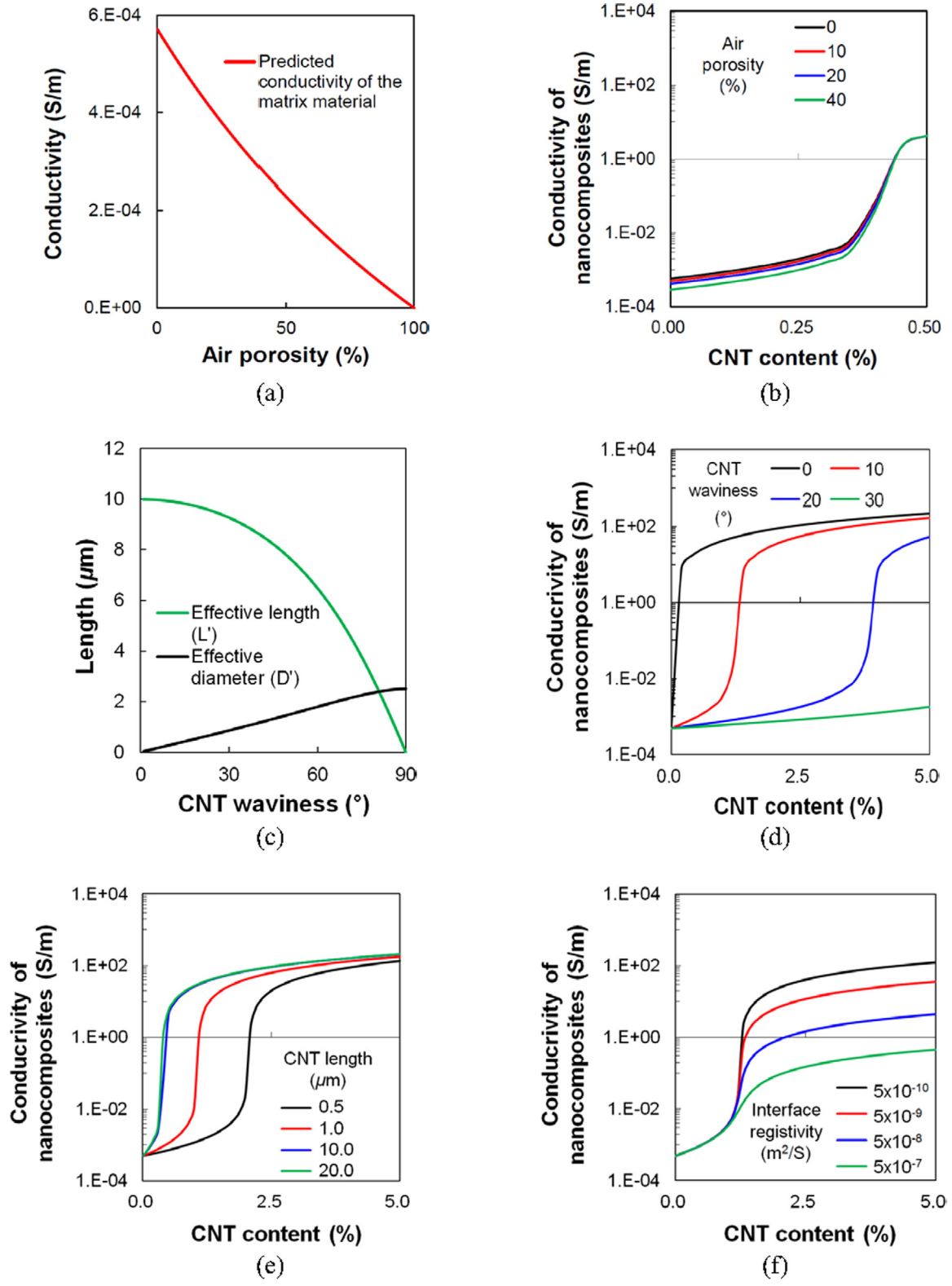

Fig. 7. Results of numerical simulations conducted with varying material and model constants.

length increases. Here, all nanotubes embedded in the matrix are assumed to be curved at the same level, $\theta = 10°$. Fig. 7(f) also shows the predicted conductivity vs. the CNT content responses with various interface resistivities (ρ_i). The figure indicates that the interface resistivity significantly affects the effective electrical behavior of the composites and that the interface effect becomes more pronounced as ρ_i increases. Fig. 8 shows the correlations among length, volume fraction, curviness of CNT, and interface resistivity on the effective electrical conductivity of cementitious composites embedded by 3D randomly oriented nanotubes.

To examine the effects of the waviness and interface on the cementitious composites further, the overall contour of the electri-

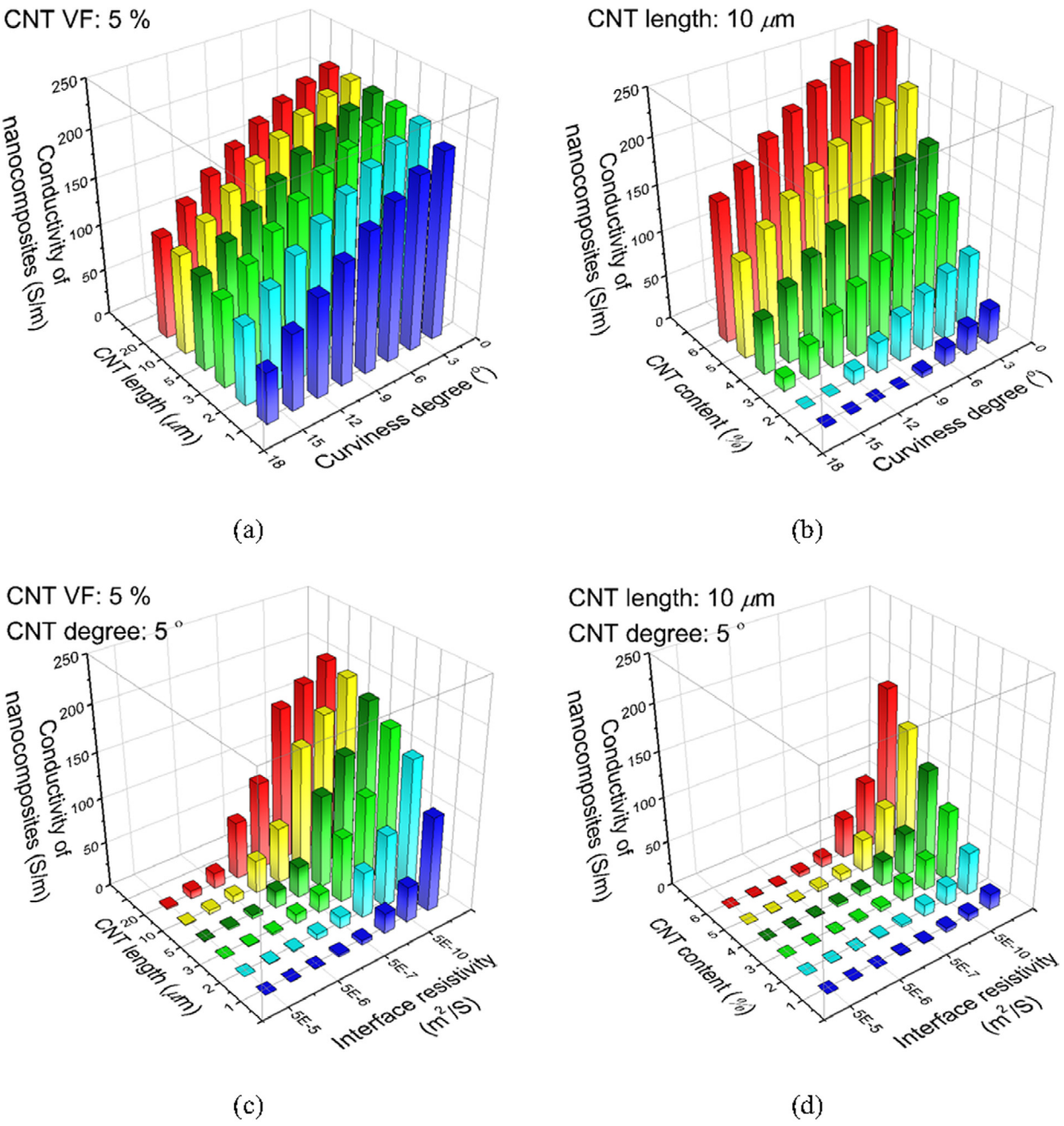

Fig. 8. Predicted overall contour of the electrical conductivity at various degrees of CNT waviness and interface resistivity.

cal performance at various degrees of waviness and the interface resistivity are plotted in Fig. 9. This figure shows that the conductivity of the cementitious composites becomes lower with increases in the CNT waviness and the interface resistivity. It also indicates that the CNT waviness has a considerable effect on the electrical properties in the range of 6–12°.

In addition, predictions based on the derived micromechanical model are compared with experimental data produced in the present study. The pore volume fractions of the composites are applied in accordance with the experimentally obtained values (Table 1), and the interface properties between nanotubes and cement are assumed to be identical in all cases ($\rho_i = 5{\cdot}10^{-8}$ m^2/s). Since the utilization of silica fume and a superplasticizer can affect the degree of CNT waviness, different values of θ are applied in accordance with the specimen type (C-CNT and F-CNT: $\theta = 11°$; P-CNT: $\theta = 9°$; PF-CNT: $\theta = 7°$). As observed in Fig. 10(a), the theoretical predictions and the experimental data are in good agreement.

Lastly, the comparison between the experimental data and the present prediction with varying the CNT content is illustrated in Fig. 10(b). Since the electrical behavior with various volume fractions of CNTs was not experimentally determined in the present study, similar material compositions of cementitious composites containing MWCNTs, silica fume, the superplasticizer, and the nylon fiber were utilized in the comparison [19,20]. The model parameters were as follows: $\phi_v = 10\%$, $\theta = 7°$, and $\rho_i = 5{\cdot}10^{-8}$ m^2/s. Fig. 10(b) shows the predicted conductivity vs. the volume fraction pertaining to the CNT relationships for the cementitious composites. Although the predicted conductivity is slightly overestimated as compared to that in the experimental observations, the simula-

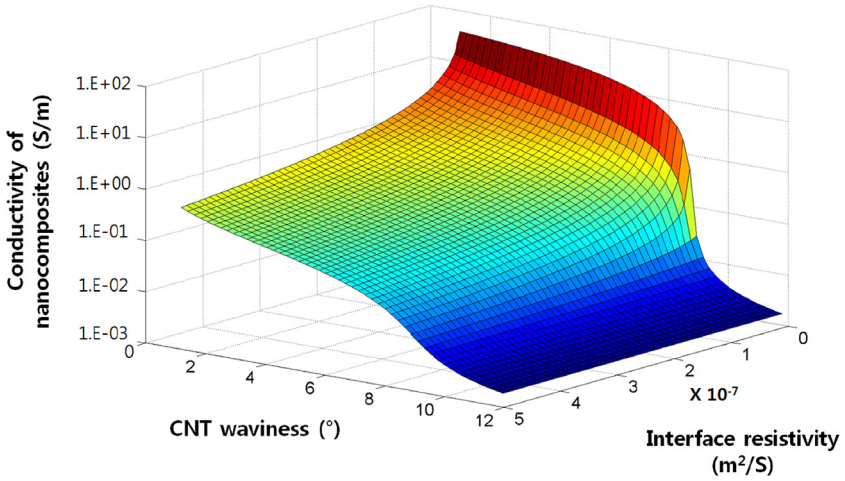

Fig. 9. The correlations among length, volume fraction, curviness of CNT, and interface resistivity on the effective electrical conductivity of cementitious composites incorporating 3D randomly oriented nanotubes.

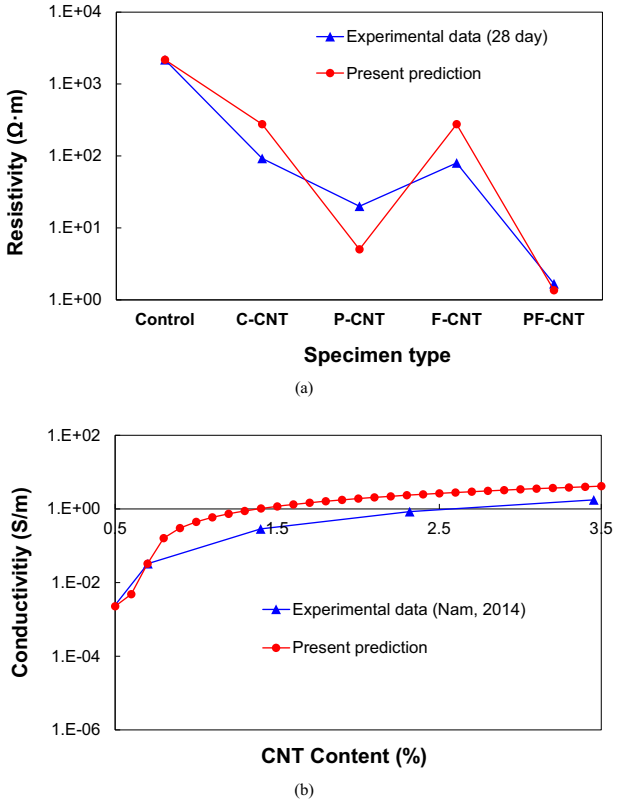

Fig. 10. Comparisons of the experimental data and the present predictions of (a) the resistivity, and (b) the conductivity of the cementitious composites.

tion and experimental results are generally in good agreement, as are the percolation thresholds.

4. Conclusions

In the present study, cementitious composites with electrical conductivity levels similar to those of a semiconductor are developed by the effective incorporation of CNT. The CNT dispersions and pore characteristics in the composites are considered to be the most important factors affecting their material performance levels. The effects of these factors were therefore intensively investigated here. A micromechanics-based model taking into account the pores and degree of CNT waviness was also proposed to predict the overall electrical performance of cementitious composites incorporating CNT. The following conclusions can be drawn considering the results of this study:

- The electrical resistivity of the cementitious composites produced from a superplasticizer and silica fume was greatly improved compared to that of Portland cement pastes and was unchanged during 28 days of curing.
- It was observed that the use of a superplasticizer can cause a loss of the vdW force among them and weaken the extent of CNT agglomeration in cementitious composites. The use of silica fume led to the transformation of a large pore (>1.0 μm) into a small pore (<0.01 μm), which decreased the variation of the electrical resistivity of cementitious composites incorporating CNT.
- The analysis results showed that the addition of silica fume improved the dispersion of CNT particles when a superplasticizer was used. In addition, the pore characteristics of the cementitious matrix was changed with the addition of silica fume, creating a good environment for the continuity of CNT particles.
- The present micromechanics-based model predicted that the lower degrees of the total porosity, the CNT waviness, and the interface resistivity resulted in the enhanced electrical behaviors of cementitious composites incorporating CNT.

The research highlights in the present work are the dispersion mechanism of CNT to create highly electrically conductive cementitious composites without any special equipment and the suggestion of a theoretical model which can predict the electrical behaviors of the composites with different mix proportions. Additional studies, however, are still required to ensure the long-term behavior of the composites and/or to assess the parameters used in the proposed model. These tasks are beyond the scope of the present paper, though they will be discussed in a future work.

Acknowledgements

This research was supported by a grant (16CTAP-C098086-02) from Technology Advancement Research Program (TARP) Program funded by Ministry of Land, Infrastructure and Transport of Korean government.

References

[1] Tyson BM, Abu Al-Rub RK, Yazdanbakhsh A, Grasley Z. Carbon nanotubes and carbon nanofibers for enhancing the mechanical properties of nanocomposite cementitious materials. J Mater Civ Eng 2011;23(7):1028–35.
[2] Smil V. Making the modern world: materials and dematerialization. John Wiley & Sons; 2013.
[3] Song G, Gu H, Mo YL. Smart aggregates: multi-functional sensors for concrete structures—a tutorial and a review. Smart Mater Struct 2008;17(3):033001.
[4] Alkhateb H, Al-Ostaz A, Cheng AHD, Li X. Materials genome for graphene-cement nanocomposites. J Nanomech Micromech 2013;3(3):67–77.
[5] Al-Dahawi A, Öztürk O, Emami F, Yıldırım G, Şahmaran M. Effect of mixing methods on the electrical properties of cementitious composites incorporating different carbon-based materials. Constr Build Mater 2016;104:160–8.
[6] Al-Dahawi A, Sarwary MH, Öztürk O, Yıldırım G, Akın A, Şahmaran M, et al. Electrical percolation threshold of cementitious composites possessing self-sensing functionality incorporating different carbon-based materials. Smart Mater Struct 2016;25(10):105005.
[7] Yun Q, Qin X, Lv W, He YB, Li B, Kang F, et al. "Concrete" inspired construction of a silicon/carbon hybrid electrode for high performance lithium ion battery. Carbon 2015;93:59–67.
[8] Chaipanich A, Nochaiya T, Wongkeo W, Torkittikul P. Compressive strength and microstructure of carbon nanotubes–fly ash cement composites. Mater Sci Eng A 2010;527(4):1063–7.
[9] Konsta-Gdoutos MS, Metaxa ZS, Shah SP. Highly dispersed carbon nanotube reinforced cement based materials. Cem Concr Res 2010;40(7):1052–9.
[10] Han B, Sun S, Ding S, Zhang L, Yu X, Ou J. Review of nanocarbon-engineered multifunctional cementitious composites. Compos Part A 2015;70:69–81.
[11] Stynoski P, Mondal P, Marsh C. Effects of silica additives on fracture properties of carbon nanotube and carbon fiber reinforced Portland cement mortar. Cem Concr Compos 2015;55:232–40.
[12] Azhari F, Banthia N. Cement-based sensors with carbon fibers and carbon nanotubes for piezoresistive sensing. Cem Concr Compos 2012;34(7):866–73.
[13] Singh AP, Gupta BK, Mishra M, Chandra A, Mathur RB, Dhawan SK. Multiwalled carbon nanotube/cement composites with exceptional electromagnetic interference shielding properties. Carbon 2013;56:86–96.
[14] Kim HK, Nam IW, Lee HK. Enhanced effect of carbon nanotube on mechanical and electrical properties of cement composites by incorporation of silica fume. Compos Struct 2014;107:60–9.
[15] Groover MP. Fundamentals of modern manufacturing: materials processes, and systems. John Wiley & Sons; 2007.
[16] Weng GJ. A dynamical theory for the Mori-Tanaka and Ponte Castañeda-Willis estimates. Mech Mater 2010;42(9):886–93.
[17] Wang Y, Weng GJ, Meguid SA, Hamouda AM. A continuum model with a percolation threshold and tunneling-assisted interfacial conductivity for carbon nanotube-based nanocomposites. J Appl Phys 2014;115(19):193706.
[18] Duan HL, Karihaloo BL. Effective thermal conductivities of heterogeneous media containing multiple imperfectly bonded inclusions. Phys Rev B 2007;75(6):064206.
[19] Nam IW, Lee HK, Sim JB, Choi SM. Electromagnetic characteristics of cement matrix materials with carbon nanotubes. ACI Mater J Am Concr Inst 2012;109(3):363.
[20] Nam IW. Electromagnetic wave shielding/absorbing characteristics of CNT embedded cement composites [Ph.D. thesis]. Korea Advanced Institute of Science and Technology (KAIST); 2014.
[21] Biro LP, Khanh NQ, Vertesy Z, Horvath ZE, Osvath Z, Koos, et al. Catalyst traces and other impurities in chemically purified carbon nanotubes grown by CVD. Mater Sci Eng C 2002;19(1):9–13.
[22] Kim GM, Naeem F, Kim HK, Lee HK. Heating and heat-dependent mechanical characteristics of CNT-embedded cementitious composites. Compos Struct 2016;136:162–70.
[23] Cao J, Chung DDL. Electric polarization and depolarization in cement-based materials, studied by apparent electrical resistance measurement. Cem Concr Res 2004;34(3):481–5.
[24] Han B, Zhang K, Yu X, Kwon E, Ou J. Electrical characteristics and pressure-sensitive response measurements of carboxyl MWNT/cement composites. Cem Concr Compos 2012;34(6):794–800.
[25] Monzó J, Paya J, Borrachero MV, Córcoles A. Use of sewage sludge ash (SSA)-cement admixtures in mortars. Cem Concr Res 1996;26(9):1389–98.
[26] Kim GM, Jang JG, Naeem F, Lee HK. Heavy metal leaching, CO_2 uptake and mechanical characteristics of carbonated porous concrete with alkali-activated slag and bottom ash. Int J Concr Struct Mater 2015;9(3):283–94.
[27] Toutanji HA, El-Korchi T. The influence of silica fume on the compressive strength of cement paste and mortar. Cem Concr Res 1995;25(7):1591–602.
[28] Nochaiya T, Chaipanich A. Behavior of multi-walled carbon nanotubes on the porosity and microstructure of cement-based materials. Appl Surf Sci 2011;257(6):1941–5.
[29] Barralet JE, Gaunt T, Wright AJ, Gibson IR, Knowles JC. Effect of porosity reduction by compaction on compressive strength and microstructure of calcium phosphate cement. J Biomed Mater Res 2002;63(1):1–9.
[30] Vaisman L, Wagner HD, Marom G. The role of surfactants in dispersion of carbon nanotubes. Adv Colloid Interface Sci 2006;128:37–46.
[31] Feldman RF, Cheng-Yi H. Properties of Portland cement-silica fume pastes I. Porosity and surface properties. Cem Concr Res 1985;15(5):765–74.
[32] Collins F, Lambert J, Duan WH. The influences of admixtures on the dispersion, workability, and strength of carbon nanotube–OPC paste mixtures. Cem Concr Compos 2012;34(2):201–7.
[33] El-Enein SA, Kotkata MF, Hanna GB, Saad M, El Razek MA. Electrical conductivity of concrete containing silica fume. Cem Concr Res 1995;25(8):1615–20.
[34] Salem TM, Ragai SM. Electrical conductivity of granulated slag–cement kiln dust–silica fume pastes at different porosities. Cem Concr Res 2001;31(5):781–7.
[35] Oertel T, Hutter F, Helbig U, Sextl G. Amorphous silica in ultra-high performance concrete: first hour of hydration. Cem Concr Res 2014;58:131–42.
[36] Mori T, Tanaka K. Average stress in matrix and average elastic energy of materials with misfitting inclusions. Acta Metall 1973;21(5):571–4.
[37] Pan Y, Weng GJ, Meguid SA, Bao WS, Zhu ZH, Hamouda AMS. Percolation threshold and electrical conductivity of a two-phase composite containing randomly oriented ellipsoidal inclusions. J Appl Phys 2011;110(12):123715.
[38] Landau LD, Bell JS, Kearsley MJ, Pitaevskii LP, Lifshitz EM, Sykes JB. Electrodynamics of continuous media, vol. 8. Elsevier; 1984.
[39] Fiedler B, Gojny FH, Wichmann MH, Nolte MC, Schulte K. Fundamental aspects of nano-reinforced composites. Compos Sci Technol 2006;66(16):3115–25.
[40] Yanase K, Moriyama S, Ju JW. Effects of CNT waviness on the effective elastic responses of CNT-reinforced polymer composites. Acta Mech 2013;224(7):1351–64.
[41] Stewart J. Multivariable calculus. Nelson Education; 2015.
[42] Nan CW, Birringer R, Clarke DR, Gleiter H. Effective thermal conductivity of particulate composites with interfacial thermal resistance. J Appl Phys 1997;81(10):6692–9.
[43] Hashemi R, Weng GJ. A theoretical treatment of graphene nanocomposites with percolation threshold, tunneling-assisted conductivity and microcapacitor effect in AC and DC electrical settings. Carbon 2016;96:474–90.
[44] Xia X, Wang Y, Zhong Z, Weng GJ. A frequency-dependent theory of electrical conductivity and dielectric permittivity for graphene-polymer nanocomposites. Carbon 2017;111:221–30.
[45] Kim GM, Yang BJ, Ryu GU, Lee HK. The electrically conductive carbon nanotube (CNT)/cement composites for accelerated curing and thermal cracking reduction. Compos Struct 2016;158:20–9.
[46] Yang BJ, Jang J, Eem S, Kim SY. A probabilistic micromechanical modeling for electrical properties of nanocomposites with multi-walled carbon nanotube morphology. Comp Part A Appl Sci Manuf 2017;92:108–17.
[47] Yang BJ, Souri H, Kim Sunghwan, Ryu Seunghwa, Lee HK. An analytical model to predict curvature effects of the carbon nanotube on the overall behavior of nanocomposites. J Appl Phys 2014;116(3):033511.
[48] Yang BJ, Cho KJ, Kim GM, Lee HK. Effect of CNT agglomeration on the electrical conductivity and percolation threshold of nanocomposites: A micromechanics-based approach. Comput Model Eng Sci 2014;103(5):343–65.